CURVATURE AND THE GLOBAL STRUCTURE OF INTERFACES IN SURFACTANT-WATER SYSTEMS

S. Hyde

COLLOQUE DE PHYSIQUE
Colloque C7, supplément au n°23, Tome 51, 1er décembre 1990

CURVATURE AND THE GLOBAL STRUCTURE OF INTERFACES IN SURFACTANT-WATER SYSTEMS

S.T. HYDE

Department of Applied Mathematics, Research School of Physical Sciences, Australian National University, Box 4, Canberra ACT 2601, Australia

Résumé-La contrainte globale spatiale imposée par la composition d'un système binaire surfactant-eau peut être exprimée en fonction de la géométrie locale intrinsèque du film de surfactant, si le film est supposé suffisamment homogène, c'est à-dire de faible énergie de courbure. Ces relations sont calculées pour des géométries (quasi-)homogènes hyperboliques, elliptiques (sphères) et parabolique (cylindres). Il est suggéré que la cristallinité de certaines mésophases de surfactants est le résultat de la contrainte homogène. Une théorie détaillée des structures rencontrées dans les phases cubiques bicontinues, ainsi que des techniques expérimentales pour déterminer la microstructure de ces phases est présentée.

Abstract-The global spatial requirement set by the composition of a binary surfactant-water system can be expressed as a function of the local intrinsic geometry of the surfactant film, assuming a reasonably homogeneous film, which is equivalent to a film of low bending energy. These relations are calculated for (quasi-)homogeneous hyperbolic, elliptic (spheres) and parabolic (cylinders) geometries. It is suggested that the crystallinity of some surfactant mesophases is a resut of the homogeneity constraint. Detailed theory of structures found in bicontinuous cubic phases, as well as experimental techniques for deciphering the microstructure of these phases is presented.

1. INTRODUCTION

In order to understand the structures of self-assembled systems, we must first attempt to delineate as full an ensemble of surfaces as possible, together with some measure of their likelihood as interfaces within surfactant mixtures. This task is a very complex one, and the variety of phase behaviour in surfactant systems is a reflection of that complexity. For now we confine our analyses to what we call *homogeneous* surfaces. These are intersection-free two-dimensional orientable surfaces free of self-intersections (embeddings) whose surface curvatures are as uniform as possible within the geometry.Since the work of Riemann we know that there are three possible geometries: elliptic (positive Gaussian curvature),parabolic (zero Gaussian curvature), and hyperbolic (negative Gaussian curvature). (For an introduction to the ideas of Riemann, see ref. [1]. Every patch of a surface must lie within one of these classes. In general, the local curvatures vary from patch to patch over the surface. We must distinguish between the geometry of the patch - the *local* geometry, which is the domain of *differential geometry*, and the *global* structure, which is the domain of *topology*. In general, it is impossible to deduce anything of the global structure from the local geometry. For example, the relative volumes on either side of an (oriented) minimal surface need not be equal. Yet, any surface patch on a minimal surface is equally curved in both directions, with no hint of the global asymmetry (for other examples, see [2]. However, if the interface is sufficiently homogeneous, approximate estimates of the surface's global characteristics can be made. These estimates are exact if the surface is perfectly homogeneous. For example, the surface to (interior) volume ratios of spheres and cylinders can be determined from the values of the (constant) Gaussian and mean curvatures alone.

The variety of interactions in surfactant-water systems can be conveniently subsumed into a phenomenological (internal surface) bending energy, related to the interfacial curvatures (the intrinsic) geometry, of the surfactant interface [3]. In the absence of significant long-range interactions the equilibrium structure of an actual surfactant/solvent mixture is that

which minimises this surface energy, as well as bulk energy contributions. The surface energy contribution will be minimised when the interfacial shape is exactly that taken up by a surfactant film in the absence of all global constraints. This ground state is the preferred local configuration. Curvature deviations away from this locally preferred shape will incur a bending energy cost, while homogeneous interfaces whose curvatures match those preferred values will be absolutely favoured. The existence of this bending energy allows us to draw connections between the local and global structures, since the preferred global structure is expected to be the most homogeneous global realisation of the local patch, provided thermal energy content of the system is not too large.

Which surfaces must be included in this analysis? At the crudest level of classification, elliptic, parabolic and hyperbolic surfaces. Since the surfaces must be as close to homogeneous as possible, the Gaussian curvature is assumed to be constant, so that the integral curvature of the surface (contained within a certain volume) is given by:

$$\int K.A = \overline{K}.A \qquad (1)$$

which means that the topology, denoted by the genus (within that volume) g, can be conveniently written by the Gauss-Bonnet theorem [4]:

$$\int\int K\,da = 2\pi(2-2g) \quad \text{or} \quad g = 1-\frac{\overline{K}.A}{4\pi} \qquad (2)$$

This link between surface geometry and topology suggests that we use the surface genus (which must be a non-negative integer) as a means to systematically generate a full catalogue of surface structures [5].

The lowest possible value of the genus - zero - can be homogeneously achieved by a sphere, which is the only homogeneous embedded elliptic candidate. Less homogeneous examples of genus zero surfaces include ellipsoids.

Surfaces of genus one have vanishing Gaussian curvature, and thus encompass all parabolic shapes. Homogeneous examples within this class are planes and cylinders*.

If the genus of an interface exceeds unity, the Gaussian curvature must be negative, so that all such surfaces are hyperbolic. Global realisations of hyperbolic interfaces are only now being deduced. Recent discoveries of minimal and constant mean curvature surfaces - such as the spectacular examples of Costa [6], Hoffman and Meeks [7], and the beautiful surfaces discovered by Pinkall and Sterling [8] - suggest the range of shapes still to be found. For this reason, it is speculative at this stage to suggest the global forms of the most homogeneous hyperbolic interfaces. It is certain that the mean and (negative) Gaussian curvatures cannot be simultaneously constant without unphysical self-intersections [9].

The best known hyperbolic interfaces are minimal surfaces, whose mean curvature vanishes everywhere on the surface. Our vocabulary of minimal surfaces includes complete non-periodic surfaces, and one two and three- periodic surfaces (whose equivalent lattice points define one two and three dimensional lattices). The presence of catenoidal or planar ends in all but three-periodic surfaces results in significant regions of low curvature, which disfavour these surfaces. (For example, while usual images of the catenoid suggest a reasonably smooth surface, the global surface contains is less homogeneous, see [10].) Of known surfaces of constant (but nonzero) mean curvature, two-periodic surfaces appear to be the most homogeneous. On these speculative grounds, we confine our investigation to these two surface types as structural candidates within our catalogue of hyperbolic surface shapes, i.e. those surfaces of genus higher than two.

A periodic surface of genus two (per unit cell) can be constructed by embedding a "wagon wheel" surface containing four spokes or tunnels within a cube, and reflecting the surface in all vertical faces to give a square network (figure 1(a)). The genus of this cell is that of the surface embedded in the three-torus, which is obtained by "gluing" all surface points separated by a lattice vector (an edge) of the cubic cell. Such an interface can adopt a range of mean curvatures (figure 1), including the examples of constant mean curvature first analysed by Lawson [11].

---

* For the sake of simplicity we assume that the genus is always equal to $(1-1/2\chi)$ where χ is the Euler characteristic.

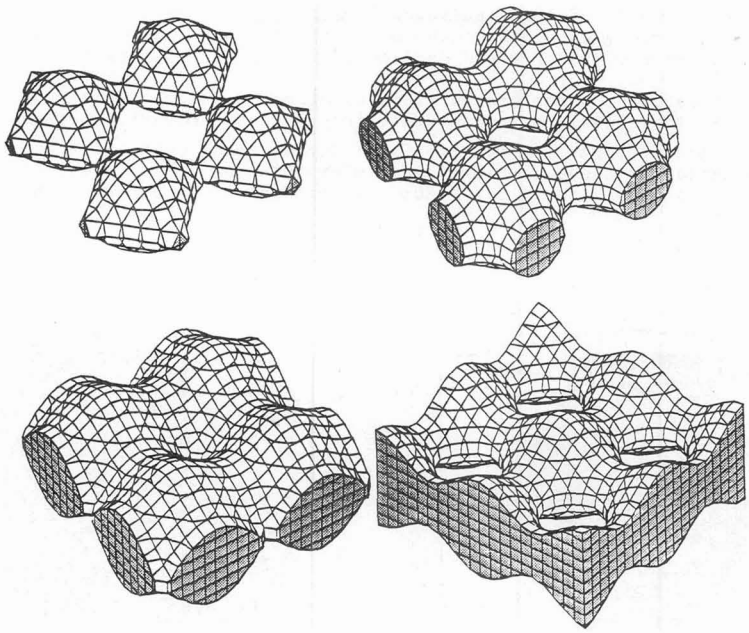

Figure 1: A variety of mesh surfaces of varying mean curvature.

In fact, similar shapes (made up of intersecting rods) were first mooted by Luzzati, as candidate structures for lipid mesophases [12, 13] and more recent studies also suggest topologically similar surfaces in other surfactant systems [14, 15]. It is important to note that these surfaces must have non-zero (average) values of mean curvature, so that they cannot be minimal surfaces. The most homogeneous global embeddings of these surfaces are parallel stacks of these surfaces, with holes of one layer lying over nodes of its neighbouring layers, resulting in a global morphology similar to the classical lamellar phase. An example is the hexagonal genus two surface, which can be uniformly stacked to give a global structure of three-dimensional rhombohedral symmetry.A body-centred tetragonal example is shown in figure 2.

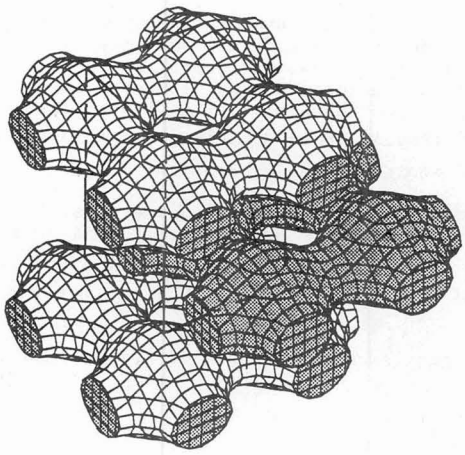

Figure 2: A homogeneous global embedding of square mesh surfaces, forming a three dimensional lattice of body-centred tetragonal symmetry.

A range of two-periodic examples exist, whose inner tunnel networks define periodic two-dimensional graphs. We call such surfaces "mesh" surfaces, in keeping with the two-

dimensional networks formed inside the surfaces. An infinite number of mesh surfaces can be designed, enclosing a variety of planar networks. Nets of higher coordination than those of hexagonal (three) and square (four) yield surfaces of genus per unit cell larger than two.

Surfaces of genus three and upwards are sufficiently topologically complex to define three-dimensional networks. The classic examples are triply periodic minimal surfaces, of genus three per unit cell and upwards [16]. These surfaces divide space into two topologically equivalent interpenetrating tunnel networks. We refer to these surfaces as "strut" surfaces. The simplest example to visualise is the P-surface, discovered by Schwarz last century (figure 3) [17].

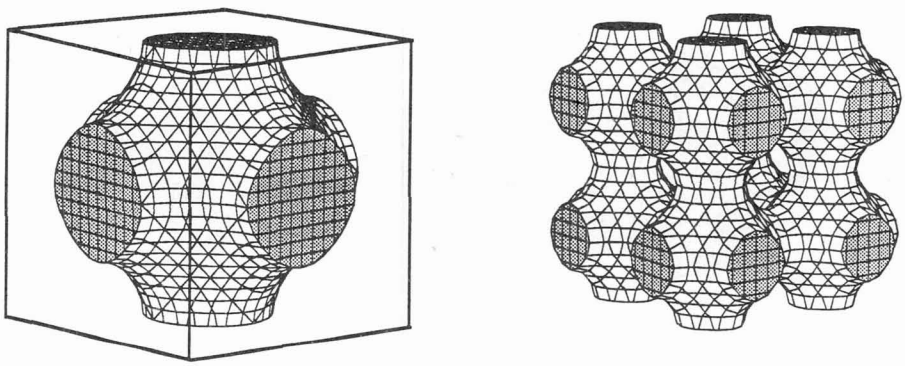

Figure 3: A schematic drawing of a conventional unit cell of the simplest infinite periodic minimal surface (IPMS), known as the P-surface#, together with a view of 8 unit cells.

Many other minimal surfaces of genus three are now known to exist, thanks to the work of Riemann (the D-surface) [18], and more recent studies by Schoen [19], Lidin [20, 21], von Schnering and Nesper [22], Koch and Fischer [23, 24]. The analysis presented by A. Fogden at this workshop suggests that the catalogue of genus three minimal surfaces is now close to complete (see Fogden, this workshop), although many more (irregular) surfaces (of higher genus) remain to be discovered. The geometry of these surfaces can be discerned by construction of a balanced patch in the assymmetric unit of the space group, leading to exact parametrisation via the Weierstrass representation [25], (Fogden, this workshop), or more approximate equipotential calculations [22], or truncated equipotential expressions [26].

Among cubic IPMS alone, a wide variety of topologies are possible. For example, surfaces of space group symmetry Im3m include the I-WP surface (first discovered by Schoen), of genus four per primitive unit cell (and nine per conventional cubic cell) [19]; the genus nine Neovius surface [27] and the O,C-TO surface of Schoen [27], which has a genus of ten per unit cell.

We can draw up the following provisional catalogue of homogeneous surface shapes:

The computer surface drawings in this article are actually trigonometric approximations to constant curvature surfaces. For more information on these representations of minimal surfaces, see I.S. Barnes et al. this conference. I thank Ian Barnes for leaving his equipotential calculation program in Canberra.

Table I: Catalogue of the most homogeneous surfaces by topological class. (The surfaces of genus >3 are representative only. Many remain to be characterised.
*These entries refer to the genus per unit cell of the surface.

Geometric class	topology (genus)	global shape	symmetry
elliptic	0	sphere	
parabolic	1	cylinder plane	
hyperbolic	2*	mesh surfaces:	
(figure 2)		square mesh	tetragonal
		hexagonal mesh	rhombohedral
	3*	strut surfaces:	
(figure 3)		P-surface	cubic (Im3m)
		gyroid	"
(Ia3d)			
		D-surface	" (Pn3m)
		H-surface	hexagonal
		T-,CLP surface	tetragonal
(figure 4)	4*	I-WP surface	cubic (Im3m)
(figure 5)	9*	Neovius surface	cubic (Im3m)
	10*	O,C-TO surface	cubic (Im3m)

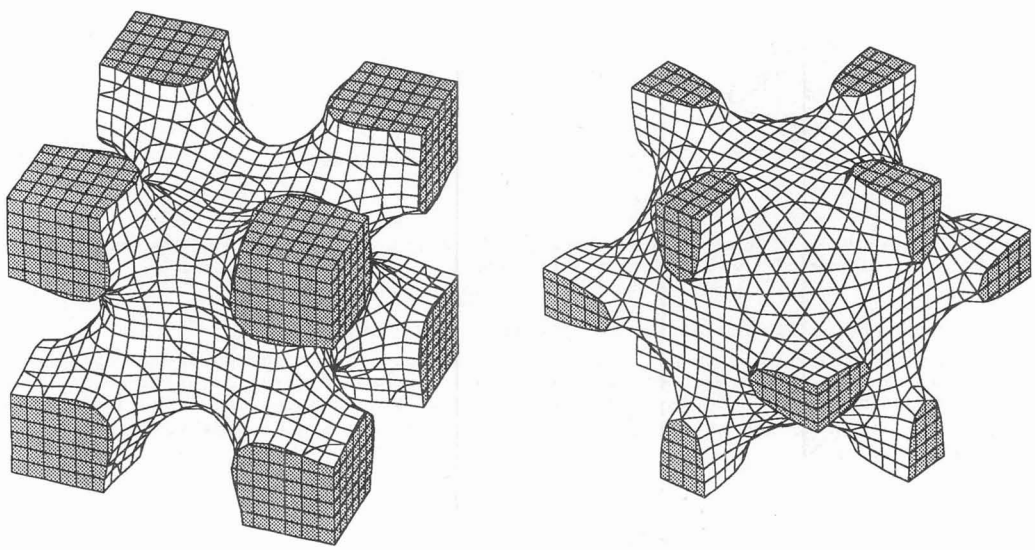

Figure 4 (left): Conventional unit cell of an approximation to the I-WP periodic minimal surface.
Figure 5 (right): Conventional unit cell of an approximation to the Neovius surface, a cubic periodic minimal surface.

2. A SIMPLE GEOMETRIC MODEL OF SELF-ASSEMBLY

Given the range of possible microstructures presented in the preceding table, we now investigate the conditions required for formation of these various interfaces in surfactant/water mixtures.

Due to the immiscibilty of surfactant chains with water, above the critical micelle concentration the surfactant molecules spontaneously associate, in order to isolate the hydrophobic chains from water. The geometry of the resulting surfactant aggregates can be described by the structure of the interface between the polar region (which consists of water and surfactant head-groups) and the hydrophobic region. At the simplest level of approximation, the (assumed molten) surfactant chains within the interfacial aggregate can be described by an average molecular shape. This shape is characterised by the "surfactant parameter", which is equal to v/al, where v is the chain volume, a the interfacial area per surfactant molecule at the hydrophobic-polar interface, and l is the chain length normal to the interface [28, 29]. Since the chains must pack to leave no area exposed to water, the curvatures of the interface are dependent on the value of the surfactant parameter. (We assume that the surfactant head-group volume is small compared with the chain volume, and the head-groups do not influence the chain aggregation.) The relation between the molecular shape, the surfactant parameter and the curvature of the aggregated interface is shown in figure 6.

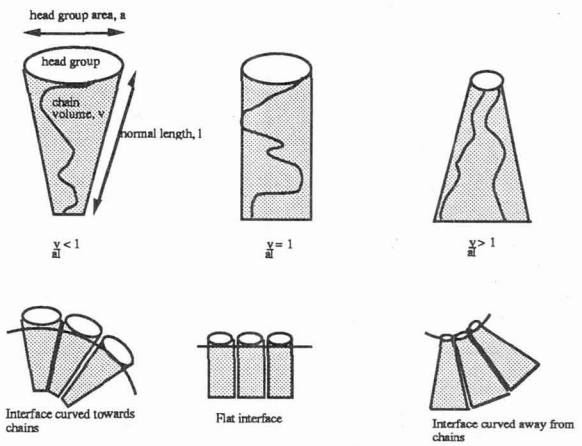

Figure 6: Schematic view of the relation between the surfactant parameter, the molecular shape, and the curvature of the surfactant interface.

If the surfactant chains lie normal to the interface (and simulations suggest that this is the case [30]) the chain ends lie on parallel surfaces separated from the polar-hydrophobic interface by a distance l. The area of surface which is formed by parallel displacement from an interfacial patch of area a(0) is related to the separation between the interface and the parallel surface patch, ξ, and the Gaussian and mean curvatures of the basal interfacial patch, K and H (figure 7).

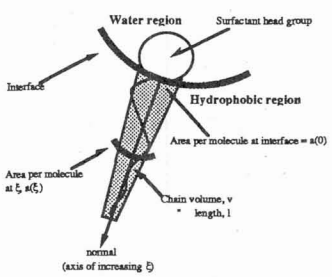

Figure 7: The relation between the surfactant chain volume and the foliation of parallel surfaces, separated from the polar-hydrophobic interface by a distance ξ.

The relation can be written [4]:

$$a(\xi) = a(0)\,[1+2H\xi+K\xi^2] \qquad (3)$$

The sign of the parallel displacement, ξ, is negative if the displacement is towards the closest centre of curvature, positive otherwise. The volume occupied by a surfactant chain is the foliation of parallel surfaces, from the interface up to the parallel surface at the free chain ends (figure 7). This chain volume is equal to:

$$v = \int_0^l a\,[\,1+2H\xi+K\xi^2]\,d\xi \quad \text{so that} \quad \frac{v}{al} = 1+Hl+\frac{Kl^2}{3} \qquad (4)$$

Equation (4) describes the value of the surfactant parameter in terms of the implicit local geometry at the polar-hydrophobic interface. Note that the chain length, l, is a natural length scale of the curvatures. The surfactant parameter is thus a measure of the preferred *local* geometry of the surfactant interface, and constrains the values of the interfacial curvatures to accommodate the molecular dimensions of the surfactant molecules.

The actual *global* shape formed by a homogeneous sweeping out of this local surface patch must partition space into the relative volumes needed to contain the (incompressible) polar and hydrophobic moieties. These volumes (on the inside and outside of the interface(s)) depend on the *composition* of the surfactant mixture. Thus, the surfactant parameter (v/al) and the composition (characterised by the chain volume fraction in the mixture, Φ) can be viewed as canonical variables which determine the global and local structures of the surfactant interface.

For a general surface, there is no connection between the intrinsic geometry of an interface, and its global form. However, a link between global and local geometry rests on the observation that the volume (inner and/or outer) formed by a perfectly homogeneous interface is that defined by all parallel surfaces on the inner/outer side of the interface up to the nearest centre of curvature. The surfaces traced out by the centres of curvature to an interface are the focal or pedal surfaces [4]. If the surface is homogeneous, the focal surface is identical to the parallel surface displaced from the interface by a separation R, where R is the (smaller) radius of curvature on that side of the interface. Thus the volume associated with a surface can be calculated by summing over all parallel surfaces to the centre of curvature. So, if the interface is sufficiently homogeneous, the extrinsic and intrinsic geometries are linked. In other words, if the surfactant interface is sufficiently homogeneous, the surfactant parameter is dependent on the composition. In the rest of this section we derive estimates of the relations between these local and global variables for the range of surfaces catalogued in Table I.

Spheres (g=0)

Since elliptic surfaces are curved exclusively towards the interior volume created by the surface, the exterior volume is independent of the intrinsic surface geometry. (The outer volume associated with a sphere is dependent on the density of spheres.) We assume that the outer volume can be considered as a foliation of parallel surfaces (i.e. larger, concentric spheres). This can only be an approximation, since these spheres cannot fill space without overlap or voids between the spheres.

Consider spherical micelles enclosing the surfactant chains, embedded in a water (plus head-group) matrix. Since the mean and Gaussian curvatures of a sphere are equal to $1/R$ and $1/R^2$ respectively, the surfactant parameter is given by equation (4):

$$\frac{v}{al} = 1 - \frac{R}{R} + \frac{R^2}{3R^2} = \frac{1}{3} \qquad (5)$$

irrespective of the surfactant concentration. In order for surfactants to form spherical micelles, this value of the parameter must be adopted by the chains. This constraint is well known [28].

If the surfactant molecules aggregate to form the complementary structure: reverse spherical micelles filled with water, the value of the surfactant parameter must vary with the concentration of the surfactant-water mixture. From equation (4), the surfactant parameter is related to the sphere radius, assuming that the chains lie on the set of exterior parallel surfaces to the sphere:

$$\frac{v}{al} = 1 + \frac{1}{R} + \frac{l^2}{3R^2} \quad \text{so that} \quad \frac{1}{R} = \frac{3}{2}\left(\sqrt{1+\frac{4}{3}\left(\frac{v}{al}-1\right)} - 1\right)$$

The chain and polar volumes related to a surface patch of area A are equal to:

$$V_{chain} = Al[1+\frac{l}{R}+\frac{l^2}{3R^2}] \quad \text{and} \quad V_{polar} = \frac{AR}{3}$$

Thus the polar volume fraction is related to the surfactant parameter by:

$$\Phi = \frac{\frac{9}{2}(\sqrt{1+\frac{4}{3}(\frac{v}{al}-1)}-1)}{1+\frac{9}{2}(\sqrt{1+\frac{4}{3}(\frac{v}{al}-1)}-1)} \qquad (6)$$

Cylinders (g=1)

The surfactant parameter required for formation of cylindrical micelles can be exactly determined, since the inner volume associated with a cylinder is perfectly homogeneous. Inserting the values of the mean and Gaussian curvatures for a cylinder (whose radius is equal to the surfactant chain length, l) into equation (4) gives:

$$\frac{v}{al} = 1 - \frac{R}{2R} + \frac{0}{3R^2} = \frac{1}{2} \qquad (7)$$

The approximate relation for the outer volume is:

$$\frac{v}{al} = 1 + \frac{l}{2R} \quad \text{and} \quad V_{chains} = Al(1+\frac{l}{2R}) \,,\; V_{polar} = \frac{AR}{2} \qquad (8)$$

This gives the relation between the composition of the mixture and the surfactant parameter:

$$\Phi = \frac{4(\frac{v}{al}-1).\frac{v}{al}}{1+4(\frac{v}{al}-1).\frac{v}{al}} \qquad (8)$$

Hyperbolic Interfaces (g>1)

The links between the molecular shape and the composition of the surfactant system are less obvious for hyperbolic shapes, since general formulae for surface area and enclosed volumes are not available. However, the technique outlined above can be used to derive exact relations for (unrealisable) homogeneous hyperbolic interfaces. The applicability of these calculations to quasi-homogeneous hyperbolic interfaces can be checked for a few well characterised hyperbolic surfaces.

For example, data are available for periodic minimal surfaces, which can be utilised to gauge the accuracy of the approximation of homogeneity. Within this approximation, the dimensionless surface to volume ratio, $S/v^{2/3}$, can be derived as a function of the topology of the surface per unit cell (characterised by the genus per unit cell, g). Since the mean curvature of minimal surfaces is identically zero, the separation between the interface and its centre of curvature (on both sides of the interface) is equal to:

$$R = \sqrt{-\frac{1}{K}} \quad \text{or} \quad R = \sqrt{-\frac{A}{2\pi(2-2g)}} \qquad (9)$$

where K is the value of the Gaussian curvature of the minimal surface per unit cell, and A is the interfacial area per unit cell. (Note that since we are assuming homogeneous interfaces, the value of K is equal at all points on the surface). Formula (4) can be utilised to calculate the volume on one side of the minimal surface ($V_{1/2}$) per unit cell:

$$\frac{V}{2} = A\sqrt{-\frac{A}{2\pi(2-2g)}}\left\{1+\frac{2\pi(2-2g)}{3A}.\frac{-A}{2\pi(2-2g)}\right\} \quad \text{i.e.} \quad \frac{V}{2} = \frac{2}{3}A\sqrt{-\frac{A}{2\pi(2-2g)}} \qquad (10)$$

so that the dimensionless surface to volume ratio is equal to:

$$\frac{A}{V^{2/3}} = \left\{\frac{3\sqrt{2\pi(2g-2)}}{4}\right\}^{2/3} \qquad (11)$$

For minimal surfaces of genus three per unit cell, this ratio is estimated to be equal to 2.418 under the assumption of homogeneity. Actual values for genus three IPMS are 2.3451 for the P-surface, 2.4177 for the D-surface, and 2.4533 for the gyroid [19, 31, 32]. Clearly then, the assumption of homogeneity is reasonable for these cases, and the analytic techniques

offer good estimates of the global properties of these surfaces. Unfortunately, corresponding data for periodic mesh surfaces is not available. However, we assume that this technique also offers reasonable estimates of the local/global relations for this class of surfaces.

Mesh surfaces (g=2)

Consider first a stack of mesh surfaces whose interiors are filled with surfactant chains. This structure consists of layers of chains, studded with pores, embedded in a continuous matrix of water and surfactant head-groups. In this case, the inner focal distance must be equal to the chain length, l, so that:

$$1+2Hl+Kl^2=0 \quad \text{and} \quad \frac{v}{al}=1+Hl+\frac{Kl^2}{3} \qquad (12)$$

If the outer focal distance is denoted by y:

$$1-2Hy+Ky^2=0 \quad \text{and} \quad \frac{v_{polar}}{ay}=1-Hy+\frac{Ky^2}{3} \qquad (13)$$

where v_{pol} is the (outer) polar volume associated with a patch on the mesh interface of area a. These equations imply:

$$Hl=3(\frac{v}{al})-2 \quad \text{and} \quad Kl^2=3-6(\frac{v}{al}) \qquad (14)$$

and the ratio between the focal distances:

$$\frac{y}{l}=\frac{1}{3-6(\frac{v}{al})} \qquad (15)$$

The link between the local surfactant parameter and the global composition is thus:

$$\Phi=\frac{\frac{v}{al}}{(\frac{v}{al}+\frac{v_{polar}}{ay}\cdot\frac{-y}{l})} \qquad (16)$$

We can see from this equation that such structures require the value of the surfactant parameter to lie between 1/2 and 2/3, in order for the interface to curve towards the chains (so that the mean curvature is by convention negative).

For values of the surfactant parameter exceeding 2/3, the interface is curved towards the polar moiety, so that the interior of the mesh layers are occupied by water and surfactant head-groups. This "reverse" mesh structure contains a continuous chain matrix, interspersed with porous polar sheets.

The structural changes which occur within the mesh phase as a function of the surfactant parameter can be related to the range of mean curvatures spanned by these mesh surfaces (illustrated by the surfaces shown in figure 1). At one extreme, where the surfactant parameter is just larger than 1/2, the Gaussian curvature (per unit cell) of the interface is close to zero, while the scaled mean curvature is close to 1/2. At this point the interface consists of deformed cylinders (similar to Delaunay surfaces [33]) just meeting at their points of closest contact, and the tunnels defining the planar nets are vanishingly narrow. As the surfactant parameter increases towards 2/3, the mean curvature of the interface decreases, so that the preferred curvature towards the chains becomes less pronounced. When the surfactant parameter is identically equal to 2/3, the mean curvature vanishes, and mesh structures cannot form (since these cannot be minimal surfaces). For values of the surfactant parameter exceeding 2/3, the interface curves away from the chains and the curvature towards the polar volume increases continuously. As the magnitude of the surfactant parameter increases, the Gaussian curvature becomes increasingly negative, so that the genus (per unit volume) becomes larger. In other words, the density of pore "defects" within the layers increases.

Strut surfaces (g=3)

When the surfactant parameter is identically equal to 2/3, the formation of hyperbolic mesh interfaces is forbidden, since the mean curvature of the interface must vanish; i.e. the interface is curved equally towards both polar and hydrophobic regions. Consequently, at this value of the local molecular geometry, the interface must be a (non-planar) minimal surface.

In fact, at the level of approximation adopted for this analysis, the local/global relation for strut interfaces separating polar and hydrophobic volumes (equation 16)) is identical to

that derived above for mesh geometries, since both are approximated by homogeneous hyperbolic surfaces.

So far, we have considered only surfactant monolayer interfaces, for which the interior and exterior volumes consist of polar and chain moieties. In general, (reversed or normal) bilayer interfaces lining the surfaces in the catalogue of Table I are less favourable than monolayers, since the surfactant parameters required for the formation of the outer monolayer differ from those in the inner monolayer, resulting in additional inhomogeneities not present for monolayers. The surfactant parameters for the inner and outer monolayers are equal to:

$$\left(\frac{v}{al}\right)_{in} = 1\text{-}H1+\frac{K1^2}{3} \; ; \; \left(\frac{v}{al}\right)_{out} = 1+H1+\frac{K1^2}{3}$$

In the case where the mean curvature vanishes(minimal surfaces), the inner and outer geometries are (locally) identical, so that equal surfactant parameters can be adopted by the surfactant molecules in both monolayers. Thus, in addition to the possibility of monolayers lining minimal surfaces intermediate to normal and reversed mesh structures, we should consider surfactant bilayers (normal or reversed) lining triply periodic minimal surfaces.

Such structures are topologically identical to those introduced by Luzzati to describe cubic phases [34]. If a bilayer decorates a periodic minimal surface, the tunnels on both sides of the surface contain the polar moiety, while the minimal surface defines the centre of the bilayer; i.e. the free chain ends (figures 8 (a), (b)). This is similar to type II structures proposed by Luzzati et al. Alternatively, if a reversed bilayer is centred on the periodic minimal surface, the water and head-groups form a curved layer bisected by the minimal surface, while the chains line the two interpenetrating tunnel networks defined by the minimal surface (Luzzati type I), illustrated schematically in figure 8(a),(b).

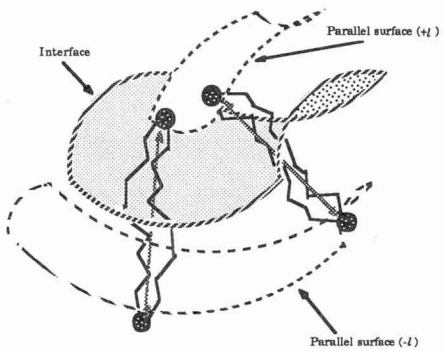

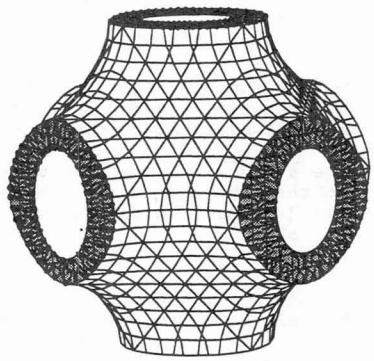

Figure 8(a) (left): Schematic picture of the arrangement of chains for curved surfactant bilayers centred on a minimal surface.

Figure 8(b) (right): Global view of the structure illustrated in figure 8(a). The water and head-groups line the two inter-penetrating tunnel networks defined by the minimal surface. (Luzzati's type II , Tiddy's V_2 phases for cubic surfaces [35])

Consider first the case of bilayers lining minimal surfaces (figure 8(a)). The chain volume fraction is related to the volumes of polar and chain moieties per unit cell (V_{pol} and V_{chain} respectively):

$$\Phi = \frac{V_{chains}}{V_{polar}+V_{chains}} = \frac{v}{a}\cdot\frac{A}{V} \qquad (17)$$

where A and V denote the head-group area per unit cell and the total cell volume.

If the chains lie normal to the interface, we can use parallel surface theory to calculate the relation between the area on the interface (which is related to a half of the total head group area, since the aggregate consists of a bilayer) and the head group area. From equation (3) this relation is:

$$S = \frac{A}{2(1+Kl^2)} \qquad (18)$$

Using the Gauss-Bonnet theorem we can relate the surface to volume ratio to the curvature and the dimensionless surface to volume ratio, $S/V^{2/3}$, written as σ, this equation can be recast:

$$\frac{\sigma^3}{(2-2g)} = \left(\frac{S}{V}\right)^2 \cdot \frac{2\pi}{K} \quad \text{or} \quad \frac{S}{V} = \sqrt{\frac{\sigma^3 K}{2\pi(2-2g)}} \qquad (19)$$

Combining equations (17)-(19) gives:

$$\Phi = 2\sqrt{\frac{\sigma^3 . Kl^2}{2\pi(2-2g)}}(1+Kl^2)\frac{v}{al} \qquad (20)$$

From equation (11) we have:

$$\sqrt{\frac{\sigma^3}{2g-2}} = 3\sqrt{\frac{\pi}{8}} \qquad (21)$$

The surfactant parameter for the molecules in the saddle-shaped bilayer is related to the Gaussian curvature at the centre of the bilayer by the equation:

$$\frac{v}{al} = \frac{v}{sl}\cdot\frac{s}{a} = \frac{(1+\frac{Kl^2}{3})}{1+Kl^2} \quad \Rightarrow \quad Kl^2 = \frac{3(1-\frac{v}{al})}{(3\frac{v}{al}-1)} \qquad (22)$$

(assuming that the scaled Gaussian curvature is small, or, equivalently, the surfactant parameter is close to one).

Inserting equations (21) and (22) into (20) yields the approximate relation between the local and global variables for bilayers lining periodic minimal surfaces:

$$\Phi = \sqrt{\frac{-12\sigma^3}{2\pi(2-2g)} \cdot \frac{\frac{v}{al}-1}{(3\frac{v}{al}-1)^3}} \cdot \frac{v}{al} \qquad (23)$$

Using equation (21), we get:

$$\Phi = \sqrt{3 \cdot \frac{\frac{v}{al}-1}{(3\frac{v}{al}-1)^3}} \cdot \frac{v}{al} \qquad (24)$$

These structures require the value of the surfactant parameter to exceed unity.

The final structural class within the catalogue of homogeneous hyperbolic aggregates consists of reversed bilayers lining periodic minimal surfaces. In this case the surfactant chains line the interpenetrating tunnel networks which are carved out by the minimal surface and the polar moiety lines the minimal surface (figure 9(a), (b)).

In this case, provided the surfactant chains lie normal to the interface, the head-groups lie on a parallel surface separated from the minimal surface by the half-thickness of the polar layer, t_p. By analogy with equation (20):

$$\Phi = 2\sqrt{\frac{\sigma^3 . Kt_p^2}{2\pi(2-2g)}}(1+Kt_p^2)\frac{v}{al}\cdot\frac{1}{t_p} \qquad (25)$$

Since

$$v = a(0)\{(t_p+1)(1+\frac{K(t_p+1)^2}{3}) - t_p(1+\frac{Kt_p^2}{3})\}$$

where a(0) is the area of minimal surface related by parallel transport to the head-group area,

$$Kt_p^2 = \frac{1-\frac{v}{al}}{(\frac{v}{al}-1)-\frac{1}{t_p}-\frac{1}{3}(\frac{1}{t_p})^2} \qquad (26)$$

Now

$$K = -\frac{1}{(t_p+1)^2} \quad \text{which implies that} \quad \frac{1}{t_p} = \frac{\frac{v}{al}-1}{\frac{2}{3}-\frac{v}{al}} \qquad (27)$$

Substituting equations (26) and (27) into (25) yields the relation between the surfactant parameter and the surfactant concentration.

$$\Phi = \sqrt{\frac{\sigma^3}{2\pi(2g-2)}} \frac{(\frac{v}{al}-1)(\frac{2}{3}\frac{v}{al}-\frac{1}{3})}{(\frac{2}{3}-\frac{v}{al})^3}.2.\frac{v}{al} \qquad (28)$$

The approximate relation for reversed bilayers on periodic minimal surfaces can be explicitly derived by substituting the surface to volume ratio estimate of equation (21).

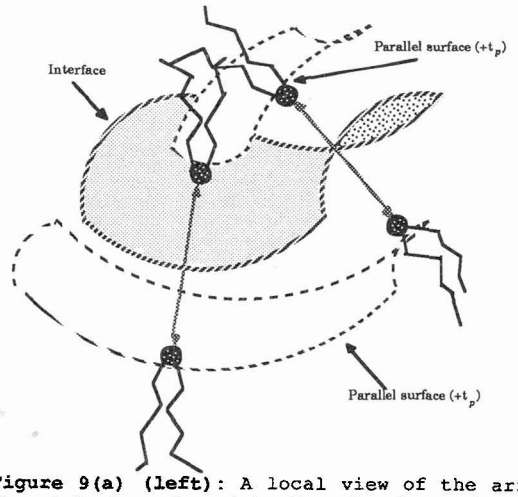

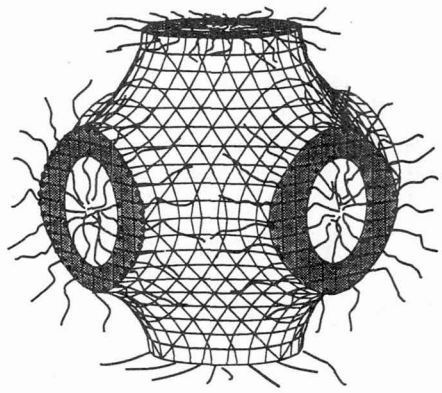

Figure 9(a) (left): A local view of the arrangement of the surfactant bilayer relative to the minimal surface interface for Luzzati type I or V_1 structures

Figure 9(b) (right): Global view of a bicontinuous bilayer phase shown in figure 9(a). The tunnel interiors are filled with surfactant chains, and the polar moiety lines the minimal surface.

3. GLOBAL GEOMETRY OF SURFACTANT INTERFACES

The catalogue of structural candidates within self-assembled systems encompasses (quasi-homogeneous) hyperbolic surfaces, as well as the better known elliptic and parabolic surfaces. The restriction of (quasi-)homogeneity has been necessary in order to compute the global characteristics of the interface from its intrinsic geometry. Geometrically, this restriction is a drastic one, and excludes many more exotic surfaces.

Within our simple model of self-assembly, the bending energy is related to the actual surfactant parameter which must be adopted by molecules within the film, v/al and the preferred (relaxed) value of the surfactant parameter, $(v/al)_0$ by:

$$F_{bend} = \kappa \{\frac{v}{al} - (\frac{v}{al})_0\}^2 \qquad (29)$$

within the harmonic approximation. Expansion of this expression in terms of the actual and preferred mean and Gaussian curvatures gives [36],

$$F_{bend} = \kappa_1 (H-H_0)^2 + \kappa_2 (K-K_0)^2 \qquad (30)$$

Analysis of the functional form of the bending energy [Fogden, Hyde and Lundberg, to be published], as well as detailed numerical simulations for nonzero spontaneous curvatures [Ennis and Marcelja, to be published] confirm this form . Note that the expression does not contain a linear term in the Gaussian curvature (except when the values of the spontaneous curvatures vanish), and the Gaussian curvature first enters into the bending energy to quadratic order.

Equation (30) demonstrates that the presence of inhomogeneities - be they mean and Gaussian curvature variations or chain length variations - give rise to a bending energy cost. (These inhomogeneities have been described as "frustrations" [37, 38].) Thus, in the absence of significant bulk energy contributions to the total free energy of a surfactant system, the homogeneous surfaces listed in Table I are expected to be of lower free energy than other, less homogeneous surfaces, and the assumption we have invoked in order to derive the global characteristics from the local geometry is precisely that required to minimise the interfacial energy. We are not concerned here with comparisons of surface free energies of the various possible interfacial geometries. (This question has been considered in ref [38]). Rather, given suitable bending moduli for the formation of these interfaces, what are the relative locations of the phases listed in Table I, and how do we account for the symmetries exhibited by surfactant mesophases?

We have remarked earlier that the exterior volumes formed by spheres and cylinders are not completely homogeneous. Thus, in the case where the chains fill this volume, the chain lengths will vary. (Alternatively, the chain lengths can be uniform, and the interface must be facetted.) The preferred state of these aggregates is that which minimises these chain length variations. These lengths can be readily calculated by the construction of Voronoi (or Dirichlet) cells about each micelle, whose volumes define that region of space closer to the micelle than to any other micelle [39]. The local/global estimates derived in the previous section are most accurate for Voronoi regions which most closely approximate spheres (for spherical reverse micelles) and cylinders (for cylindrical reverse micelles), for which the calculations are exact. In other words, the most homogeneous structures (which minimise the bending energy) are those with the largest number of faces in the Voronoi cells. Data for two and three dimensional arrays are given below.

	lattice	number of faces in Voronoi cell	
2-d	hexagonal	6	
	square	4	
3-d	body-centred cubic	14	(ref. [40])
	random close packing	13.3	(ref [41])
	cubic close packing (fcc)	12	(ref [40])

On the basis of these data, cylindrical reverse micelles are expected to pack into (2-d) hexagonal lattices, and spherical reverse micelles assemble into most homogeneous arrays by forming body-centred cubic lattices. (It is interesting to note that the random sphere packing of Bernal is close to optimal homogeneity.) Alternatively, the chain lengths can be made absolutely uniform by deformation of the cylinders to give hexagonal prisms, and facetting of the spheres to form truncated octahedra.

The bending energies for a range of global hyperbolic interfaces are more difficult to determine. According to the homogeneity criterion, mesh and strut interfaces are conjectured to be most favourable. It is relevant to note here that a strut minimal surface exhibiting 5-fold rotational symmetry arises naturally in the context of regular triply-periodic minimal surfaces. Although the presence of the 5-fold axis means that the global immersion of this surface in three-dimensional euclidean space will densely fill space, a sufficiently small curvilinear coordinate domain is expected to yield an embedded surface element in space. Thus, a collection of such elements, smoothly joined, will form a globally embedded minimal surface with some characteristics of quasicrystalline lattices. Similarly, it is possible to imagine a mesh surface, whose pores lie on a Penrose lattice. Stacks of these surfaces can be arranged to give a global structure similar to the decagonal phase found in quasicrystalline systems. These strut and mesh surfaces may well be reasonably homogeneous

compared with translationally ordered (crystalline) interfaces. However, for now, we adopt the classical assumption that crystalline surfaces are most homogeneous.

Assuming the validity of this claim, among translationally symmetric surfaces those of maximal symmetry are expected to be most homogeneous. Consequently, hexagonal and square mesh surfaces, which lead to three-dimensional rhombohedral and (body-centred) tetragonal symmetries are the most favoured interfaces of genus two per unit cell. For (strut) surfaces of genus three (and higher) per unit cell, cubic symmetries result in the most homogeneous structures.

These symmetry classes correspond to those found in many surfactant mesophases. Thus, assuming that translationally ordered surfaces have a more uniform distribution of curvatures than disordered surfaces, the formation of crystalline mesophases of rhombohedral, tetragonal and cubic symmetries can be explained as a result of minimisation of the surface (bending) energy alone.

The analyses of the previous section can be collected into a universal plot of the local molecular shape as a function of the global interfacial geometry. In order of increasing surfactant parameter, we expect spherical micelles to form at the minimum possible surfactant parameter, 1/3. Between this value and 1/2, the spheres elongate to form ellipsoids,which eventually fuse, giving cylinders (or less homogeneous Delaunay surfaces). Between values of the surfactant parameter of 1/2 and 2/3, rhombohedral or tetragonal mesh surfaces can form, consisting of planar perforated sheets of surfactant chains embedded in a continuous water and head-group matrix. Since the outer volume contains the polar moiety, the mesh spacing is free to vary, without altering the chain geometry. Thus, the surfactant parameter is independent of the concentration within this regime. (Equation (16) is applicable to homogeneous exterior volumes. Since we assume that the sole role of the polar region is to fill a volume, this is not applicable here.) For values of the surfactant parameter exceeding 2/3, the reversed mesh geometry can form, in which case the polar layers are embedded in a continuous matrix of surfactant chains. In this case then, the composition uniquely determines the surfactant chain geometry, and there is a one-to-one relation between local and global variables (expressed by equation (16)). The regions of existence of these various monolayer structures are shown in figure along with the relations for bilayer structures.

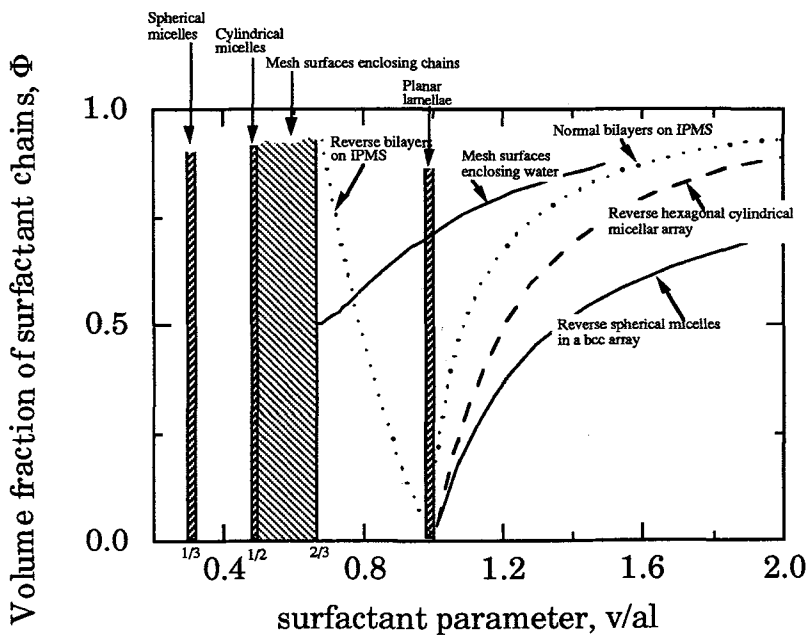

Figure 10: Plot of the relation between the local and global phases for the surfaces described in Table I.

4.STRUCTURAL VARIATION WITHIN CUBIC PHASES

A few experimental studies of the cubic phase of surfactant or lipid systems have revealed the presence of more than one interfacial structure within the region, with a first order transition between the distinct phases [42, 43, 44, 45]. So far, these observations have been confined to type II cubic phases (consisting of bilayers centred on IPMS, with water in the tunnels) for which the surfactant parameter is constrained to be larger than unity. Some feature of these observations can be understood in terms of the simple block model outlined in the previous sections.

The local/global relation for cubic phases plotted in figure 10 assume perfect homogeneity of curvatures within periodic minimal surfaces. Within this approximation, the packing index, $\sqrt{\sigma^3/(2g-2)}$, can be derived from equation (21), assuming constant mean and Gaussian curvatures over the interface, $\sqrt{\sigma^3/(2g-2)} = \sqrt{9\pi/8} = 1.8800$.

In three dimensional euclidean space, some variation of Gaussian curvature must occur over the minimal surface. Thus the assumption of homogeneity is violated and the packing index differs from 1.8800. Calculated values of the packing index for some periodic minimal surfaces are given in Table II.

TABLE II: Packing indices $(\sqrt{\sigma^3/(2g-2)})$ for a range of periodic minimal surfaces.

IPMS	genus	space group	packing index
D-surface	3	Pn3m	1.8796
I-WP surface	4	Im3m	1.8612
gyroid	3	Ia3d	1.9213
CLP surface (c/a=2)	3	$C4_2/mmc$	1.9430
P-surface	3	Im3m	1.7956
Neovius surface	9	Im3m	1.6643 (ref[19])
F-RD surface (ref[32])	6	Fm3m	1.6487

We can use these actual values of the packing index to plot the local/global relations for each IPMS, using equation (23). The plots for this limited range of surfaces are shown in figure 11.

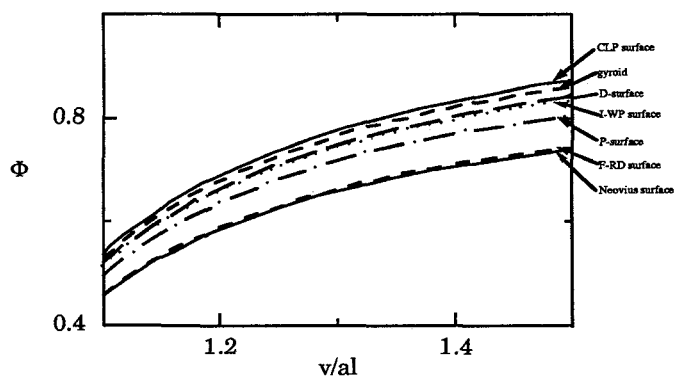

Figure 11: Variation of local and global variables for various IPMS.

The model suggests that (given a sufficiently slowly varying surfactant parameter with composition) the phases formed upon water dilution will be in order of decreasing packing index, in order to accommodate the increasing volume of water, without altering the local molecular shape significantly.

Estimates of the relative bending energy costs associated with these various IPMS can be made as follows. Since the ideal value of the packing index assumes perfect homogeneity, the difference between the actual and ideal values of the packing index reflects the degree of homogeneity of the IPMS. Using this comparison, the surfaces listed in Table III have been arranged in order of decreasing homogeneity,and increasing bending energy cost. A general trend of decreasing homogeneity with increasing genus per unit cell can be discerned, with the exception of the I-WP surface. It is interesting to note that the genus four I-WP surface* (not considered by Sadoc and Charvolin [46]) is expected to be more stable than the genus three P-surface . Although recent investigations of a pseudo-binary surfactant/water cubic phase[45] suggest that the bilayer decorates the P-surface for a phase of Im3m symmetry (which is that of both the P- and I-WP surfaces), this result is less certain for other systems. For example, structural data for the cubic phase found in the binary SDS/water system [15] (probably the best-studied system to date) is difficult to reconcile with the P-surface [47].

Since the packing index of the D-surface is closest to that of an ideal homogeneous minimal surface, the D-surface is expected to be the most stable (cubic) phase. As the rigidity of the bilayers decreases (so that they can tolerate increasingly large inhomogeneities), the progression:

D-surface (Pn3m) -> I-WP surface (Im3m)

or, for still lower rigidities:

gyroid (Ia3d)->D-surface (Pn3m)->I-WP surface (Im3m)->P-surface (Im3m).

While this simple model cannot hope to reproduce all the details of cubic phase formation, it is striking to compare the symmetries of cubic phases in surfactant/water and lipid/water systems with those listed above [48,49]. The space groups Im3m, Pn3m and Ia3d abound, and transitions from Pn3m->Im3m and Ia3d->Pn3m have been observed in a number of systems.

5.EXPERIMENTAL DETERMINATION OF MICROSTRUCTURE

Complementary to these theoretical studies of possible aggregate microstructures are experimental investigations of these phases. The principal probe of microstructure has been small angle scattering of X-rays or neutrons. Since the interfaces are usually undergoing thermal fluctuations the assignation of microstructure is very difficult. Scattering data from crystalline mesophases usually result in about a dozen Bragg reflections at best, compared with many times more reflections from atomic crystals. Ironically, despite the introduction of intense synchrotron sources, the classical X-ray investigations into lipid/water mesophases by Luzzati's group almost thirty years ago remain the definitive studies.

According to the approach espoused here, the microstructure can be characterised by the symmetry and topology per unit cell of the interface. (It is usually possible to decide whether the interface consists of monolayers or bilayers of surfactant on topological grounds [47].) The symmetry of the interface can be determined from the relative peak spacings (given a sufficient number of peaks), while the topology of the interface is directly related to the relative intensities of the peaks,which are more difficult to determine with accuracy.

For crystalline hyperbolic interfaces, we can use parallel surface theory to estimate the interfacial topology from measurements of the swelling of the unit cell as a function of composition [45]. This technique obviates the need to measure peak intensities and relies only on measurements of the peak positions as a function of the water content of the sample. The technique requires estimates of the head-group area per unit cell, A, (which can be calculated from the head-group area per surfactant molecule and the composition and the unit cell volume) and the chain length, l.

Using equation (18) together with the Gauss-Bonnet theorem, for bilayers lining an IPMS of genus g per unit cell:

* or genus seven per conventional unit cell -

$$\frac{KA}{2(1+K1^2)} = 2\pi(2\text{-}2g) \quad \therefore K = \frac{4\pi(2\text{-}2g)}{A\text{-}4\pi(2\text{-}2g)1^2} \qquad (31)$$

The dimensionless surface to volume ratio is related to the lattice parameter of the cell (assumed to be cubic for simplicity) by:

$$\sigma = \frac{S}{\alpha^2} = \frac{A}{2(1+K1^2)\alpha^2} = \frac{A}{2(1+\frac{4\pi(2\text{-}2g)1^2}{A\text{-}4\pi(2\text{-}2g)1^2})}$$

But the head-group area per unit cell is much larger than $4\pi(2\text{-}2g)1^2$, so that we can make the approximation:

$$\sigma \approx \frac{A}{2\alpha^2}(1-\frac{4\pi(2\text{-}2g)1^2}{A}) \qquad (32)$$

This equation suggests a useful "master plot". If $A/2\alpha^2$ is plotted against $2.\pi.1^2/\alpha^2$ for a range of compositions, the plot should be linear, with slope equal to (2-2g), and intercept equal to the dimensionless surface to volume ratio, σ. These two structural characteristics serve to completely specify the interfacial geometry, since the surface to volume ratio is characteristic of both the symmetry and the topology.

This technique has been used to decipher the microstructures within the cubic phase region of the (pseudo-binary) surfactant mixture consisting of the double chained cationic quaternary ammonium surfactant didodecyldimethylammonium bromide (DDAB)/cyclohexane/water. At the compositions required for formation of (room temperature) cubic phases, measurements indicate that all the alkane solvent is absorbed into the chain region, thereby swelling the hydrophobic volume and increasing the magnitude of the surfactant parameter to a value marginally larger than unity [45]. The surfactant molecular dimensions have been estimated from those inferred from measurements of the neighbouring lamellar phase [50]. The resulting master plot for a range of samples within the cubic phase region is shown in figure 12(a). The linear plot reveals at a glance the presence of two distinct structures,. Magnifications of the two regions are shown in figures 12(b) and (c). The theoretical lines for IPMS whose symmetries are those measured are also shown. The data indicate the presence of bilayers lying on the D-surface, and, at higher water content, the P-surface. It is important to note that the linear character of the plots confirm the proposed structural class, *viz.* bilayers lying on IPMS.

A similar relation between the lattice parameters and the composition can be deduced for the complementary structure, consisting of reversed bilayers lining IPMS:

$$\sigma \approx \frac{A}{2\alpha^2}(1-\frac{4\pi(2\text{-}2g)t_p^2}{A}) \qquad (33)$$

If the surfactant parameter is close to unity, the half-thickness of the polar layer, t_p, can be related to the polar volume fraction:

$$\Phi_{polar} = \frac{3t_p(1+\frac{Kt_p^2}{3})}{2(t_p+1)} \quad \text{so that} \quad t_p \approx \frac{2l.\Phi_{polar}}{(3\text{-}2\Phi_{polar})} \qquad (34)$$

This yields the approximate master plot equation:

$$\sigma = \frac{A}{2\alpha^2}(1-\frac{4\pi(2\text{-}2g)}{A}\frac{4l^2\Phi_{polar}^2}{(3\text{-}2\Phi_{polar})^2}) \qquad (35)$$

Similar relations can be derived for mesh structures, offering a useful technique to distinguish between these phases and lamellar phases (which should exhibit a linear swelling with concentration).

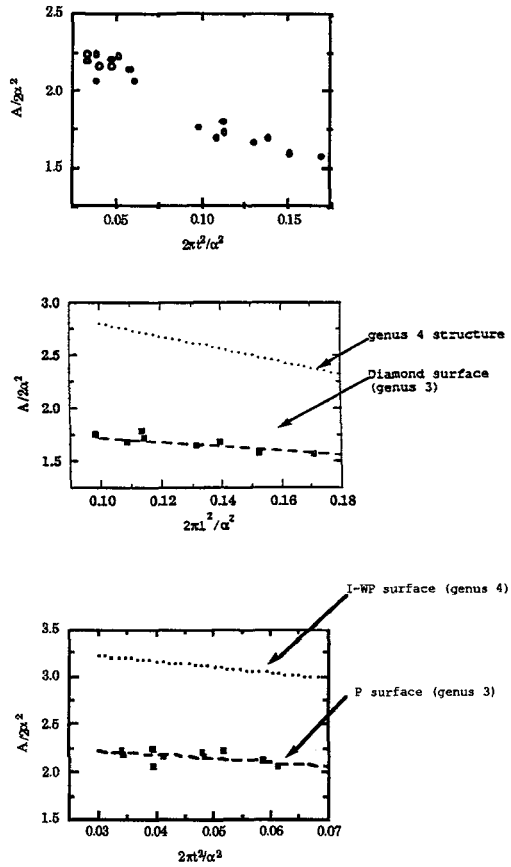

Figure 12 (from top to bottom): **(a)** Master plot, using equation (32) for cubic phase data measured in the pseudo-binary DDAB/cyclohexane/water system. A, t and α refer to the head-group area per unit cell, the (oil swollen) chain length and the cubic lattice parameter. **(b)**, **(c)**: Magnification of the two distinct region in figure 12(a).

6.CONCLUSIONS

The purpose of this paper has been to quantify the dual demands on any interfacial geometry imposed by local constraints - set by the preferred architecture of the surfactant molecules - and the global constraint set by the composition of the mixture. Under the crude assumption of fixed molecular dimensions and rigid interfaces, the plots of figures 10 and 11 are equivalent offer complete description of the phases formed as a function of these canonical variables.

Of course, surfactant molecules are not blocks of rigid architecture, and the rigidity of these films is a complex function of a range of surface forces, the usual thermodynamic variables and electrostatic interactions. The enormous variety of surfactant and lipid species encompasses the complete span of behaviour; from rigid short-chained ionic surfactants, whose molecular shape is relatively insensitive to the solution conditions (such as DDAB), to floppy nonionic polyoxyethylene molecules,whose head-groups occupy an appreciable volume compared with the chains [51]. Self-assembled structures of the former class conform best to the assumption inherent in the geometrical analysis described in this paper. The latter class are closer to block copolymers, where the preferred chain lengths and interfacial areas per molecule are set by chain entropy considerations.

It is interesting to note that the phase behaviour of copolymers in solution is qualitatively similar to that of surfactants. The rich variety of hyperbolic interfaces is only now being recognised. Just as was the case in surfactant science until a few years ago, our familiarity with elliptic and hyperbolic interfaces led to the mistaken assignation of these hyperbolic phases in terms of the more classical structures.

Recently, a bicontinuous cubic phase consisting of an interface which resembles the D-surface has been seen in block copolymer systems of both linear diblock and star diblock architectures[52, 53]. Also, recent observations indicate the phase progression from lamellar -> mesh -> strut architecture in block copolymers in solution [Hyde, Koizumi, Hasegawa and Hashimoto, in preparation]. Theoretical work suggests that these phases too can be understood from a combination of local and global constraints (whereas the locally preferred interfacial geometry is invariably elliptic for these systems). So, at both extremes of definition of the molecular shape, the aggregation behaviour exhibit common features. The presence of hyperbolic interfaces in these systems is a challenge to our powers of geometric intuition. The variety of forms found under the crude assumptions outlined here suggest the richness that will be found in nature.

REFERENCES

(1) Bonola, R. *Non-Euclidean Geometry;* Dover Publications, Inc.: New York, 1955.
(2) Hildebrandt, S. *Sonderforschungsbereich 72, preprint series* **1985**, No. 754.
(3) Helfrich, W. *Z. Naturforsch.* **1973**, *28c*, 693.
(4) Goetz, A. *Introduction to Differential Geometry;* Addison Wesley Publishing Company: Reading, Massachusetts, 1970.
(5) Hilbert, D.; Cohn-Vossen, S. *Geometry and the Imagination;* Chelsea Publishers: New York, 1952.
(6) Costa, C. *Bull. Soc. Bras. Mat.* **1984**, *15*, 47-54.
(7) Hoffman, D.; Meeks III, W. H. *J. Differential Geom.* **1985**, *21*, 109-127.
(8) Pinkall, U.; Sterling, I. *Math. Intell.* **1987**, *9*, 38-43.
(9) Willmore, T. J. in *An Introduction to Differential Geometry;* Oxford University Press, Delhi, 1985; p 137.
(10) Hoffman, D. *Math. Intell.* **1987**, *9*, 8-21.
(11) Lawson, H. B. *Ann. of Math.* **1970**, *92*, 335-374.
(12) Luzzati, V.; Gulik-Krzywicki, T.; Tardieu, A. *Nature* **1968**, *218*, 1031-1034.
(13) Luzzati, V.; Tardieu, A.; Gulik-Krzywicki, T. *Nature* **1968**, *217*, 1028.
(14) Kékicheff, P.; Tiddy, G. J. T. *J. Phys. Chem.* **1989**, *93*, 2520.
(15) Kékicheff, P.; Cabane, B. *J. Phys. France* **1987**, *48*, 1571-1583.
(16) Meeks III, W. *Bull. Am. Math. Soc.* **1977**, *83*, 134.
(17) Schwarz, H. A. Springer, Berlin, 1890;
(18) Riemann, B. in *Über die Flaeche vom kleinsten Inhalt bei gegebener begrenzung;* Dover Publications Inc., New York, 1953; see pp. 326 ff.
(19) Schoen, A. H., *Infinite periodic minimal surfaces without self-intersections,* N.A.S.A. Technical Report No. D-5541, 1970
(20) Lidin, S.; Hyde, S. T. *J. Physique* **1987**, *48*, 1585-1590.
(21) Lidin, S. *J. Phys. France* **1988**, *49*, 421-427.
(22) von Schnering, H.-G.; Nesper, R. *Angew. Chem. Int. Ed. Engl.* **1987**, *26*, 1059-1080.
(23) Fischer, W.; Koch, E. *Acta Cryst.* **1989**, *A45*, 726-732.
(24) Koch, E.; Fischer, W. *Acta Cryst.* **1990**, *A46*, 33-40.
(25) Hyde, S. T. *Z. Kristallogr.* **1989**, *187*, 165-185.
(26) Mackay, A. L. *Angew. Chem. Int. Ed. Engl.* **1988**, *27*, 849-850.
(27) Neovius, E. R. *Bestimmung Zweier Speciellen Periodische Minimalflaechen;* Frenckel & Son: Helsinki, 188.
(28) Israelachvili, J. N.; Mitchell, D. J.; Ninham, B. W. *J. Chem. Soc. Faraday Trans. 2* **1976**, *72*, 1525.
(29) Mitchell, D. J.; Ninham, B. W. *J. Chem. Soc. Faraday Trans. 2* **1981**, *77*, 601-629.
(30) Gruen, D. W. R. *J. Phys. Chem.* **1985**, *89*, 146-153.
(31) Mackay, A. L.; Klinowski, J. *Compu. & Math. Appl.* **1986**, *12B*, 803-824.
(32) Anderson, D.M., Ph.D. Thesis, University of Minnesota, 1986.
(33) Thompson, D'A. W. *On Growth and Form;* Cambridge, 1917 .
(34) Luzzati, V.; Spegt, P. A. *Nature* **1967**, *215*, 701-704.
(35) Blackmore, E.; Tiddy, G. J. T. *J. Chem. Soc., Faraday Trans. 2* **1988**, *84*, 1115-1127.
(36) Hyde, S. T.; Barnes, I. S.; Ninham, B. W. *Langmuir* **1990**, *6*, 1055-1062.
(37) Charvolin, J.; Sadoc, J.-F. *J. Phys. Chem.* **1988**, *92*, 5787.
(38) Anderson, D. M.; Gruner, S. M.; Leibler, S. *Proc. Natl. Acad. Sci. USA* **1988**, *85*, 5364-5368.
(39) Coxeter, H. S. M. *Introduction To Geometry;* John Wiley & Sons, Inc.: New York, 1969.

(40) Williams, R. *The Geometrical Foundation of Natural Structure;* Dover Publications, Inc.: New York, 1979.
(41) Bernal, J. D. *Nature* **1959**, *183*, 144-147.
(42) Larsson, K. *Nature* **1983**, *304*, 664.
(43) Hyde, S. T.; Andersson, S.; Ericsson, B.; Larsson, K. *Z. Kristallogr.* **1984**, *168*, 213-219.
(44) Caffrey, M. *Biophys. J.* **1989**, *55*, 47-52.
(45) Barois, P.; Hyde, S. T.; Ninham, B. W.; Dowling, T. *Langmuir* **1990**, *6*, 1136-1140.
(46) Sadoc, J. F.; Charvolin, J. *J. Physique* **1986**, *47*, 683.
(47) Hyde, S. T. *J. Phys. Chem.* **1989**, *93*, 1458-1463.
(48) Luzzati, V.; Mariani, P.; Gulik-Krzywicki, T. in *The physics of amphiphilic layers*, Langevin, D. Boccara, N.; Springer-Verlag, Berlin, 1987; pp 131-137.
(49) Fontell, K. *Colloid Polym. Sci.* **1990**, *268*, 264-285.
(50) Fontell, K.; Ceglie, A.; Lindman, B.; Ninham, B. W. *Acta Chem. Scand.* **1986**, *A40*, 247.
(51) Mitchell, D. J.; Tiddy, G. J.; Waring, L.; Bostock, T.; McDonald, M. P. *J. Chem. Soc., Faraday Trans. 1* **1983**, *79*, 975-1000.
(52) Thomas, E. L.; Anderson, D. M.; Henkee, C. S.; Hoffman, D. *Nature* **1988**, *334*, 598-601.
(53) Hasegawa, H.; Tanaka, H.; Yamasaki, K.; Hashimoto, T. *Macromolecules* **1987**, *20*, 1651-1662.